MIT Open Access Articles

A sensitivity study on the role of the swamps of southern Sudan in the summer climate of North Africa using a regional climate model

Massachusetts Institute of Technology

A sensitivity study on the role of the swamps of southern Sudan in the summer climate of North Africa using a regional climate model

**Modathir A. H. Zaroug · M. B. Sylla · F. Giorgi ·
Elfatih A. B. Eltahir · Pradeep K. Aggarwal**

Abstract We used the regional climate model RegCM3 to investigate the role of the swamps of southern Sudan in affecting the climate of the surrounding region. Towards this end, we first assessed the performance of a high resolution version of the model over northern Africa. RegCM3 shows a good skill in simulating the climatology of rainfall and temperature patterns as well as the related circulation features during the summer season, outperforming previous coarser resolution applications of the model over this region. Sensitivity experiments reveal that, relative to bare soil conditions, the swamps act to locally modify the surface energy budget primarily through an increase of surface latent heat flux. Existence of the swamps leads to lower ground temperature (up to 2 °C), a larger north–south temperature gradient, and increased local rainfall (up to 40 %). Of particular importance is the impact on rainfall in the surrounding regions. The swamps have almost no impact on the rainfall over the source region of the Nile in Ethiopia or in the Sahel region; however, they favor wetter conditions over central Sudan (up to 15 %) in comparison to the bare desert soil conditions.

1 Introduction

Wetlands are crucial to the global carbon cycle, water balance, wildlife, biodiversity, and human food production (Neue et al. 1997). However, more than half of the world's wetlands have vanished in the last decades for various reasons (Schuyt 2005; Turner et al. 2000).

In particular, the swamps of southern Sudan consist of three sub-basins: Bahar El Ghazal flowing eastward, Sobat flowing westward and receiving tributaries from highlands on the borders of Ethiopia, and the Sudd wetland flowing northward. These sub-basins are shown in Fig. 1, highlighted by a blue color in the lower panel. However, there is no broad agreement on the swamp size due to the difficulty of access to the area. In fact, the area of the swamp is still highly debated in recent studies.

For example, Butcher (1938) deduced from air photography that the Sudd area is about 7,200 km², while Hurst and Phillips (1938) estimated the same area of the swamp in 1931/1932 as 8,300 km². More recently, Mohamed et al. (2004) estimated the Sudd basin to extend about 38,600 km², the Sobat basin about 42,900 km² (mostly dry with some seasonal swamps), and the Bahr el Ghazal basin about 59,300 km², consisting of a mixture of swamps and

M. A. H. Zaroug (✉)
Dinder Center for Environmental Research,
Khartoum, Sudan
e-mail: modathir_23@yahoo.com

M. A. H. Zaroug · M. B. Sylla · F. Giorgi
Earth System Physics,
International Center for Theoretical Physics,
Trieste, Italy

M. A. H. Zaroug
Hydraulics Research Center,
Ministry of Water Resources and Electricity,
Wad Madani, Sudan

E. A. B. Eltahir
Department of Civil and Environmental Engineering,
Massachusetts Institute of Technology,
Cambridge, MA, USA

P. K. Aggarwal
Isotope Hydrology Section, International Atomic Energy Agency,
Vienna, Austria

Fig. 1 The domain for North Africa, where the swamps are shown in the *bottom rectangle* in south Sudan. The radiation parameters have been averaged along the *rectangles* in central Sudan and south Sudan
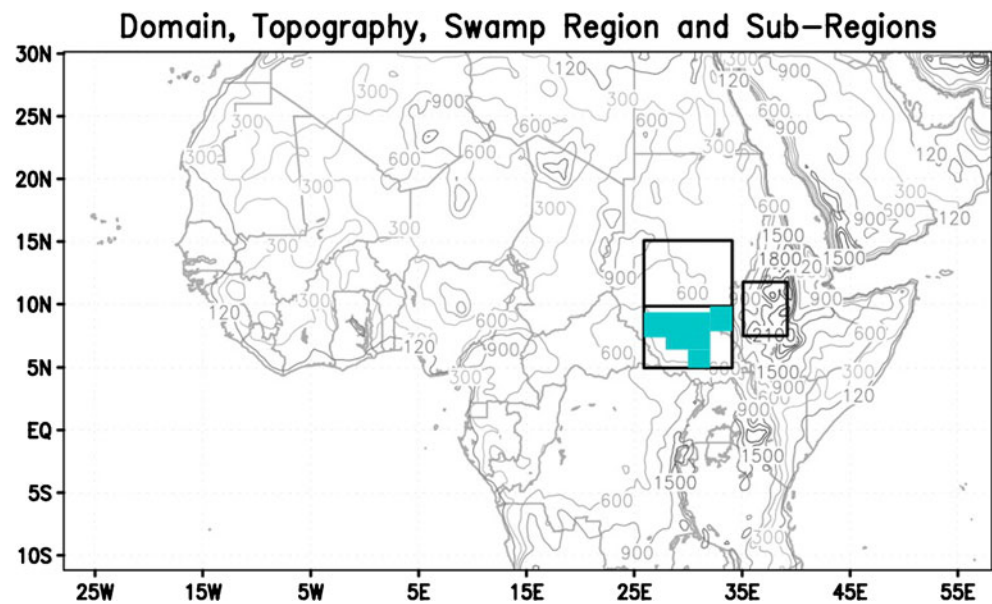
dry land. The area of Bahr el Ghazal Swamp was estimated to be 84,950 km^2 by Chan and Eagleson (1980), who assumed that it consists of papyrus swamp (16,600 km^2) and grassland (68,400 km^2), in part seasonally flooded. The total of the three sub-basins was somewhat exaggerated in this study, estimated to be about 278,300 km^2. Other recent studies attempted to estimate the area of the swamp. Using multitemporal satellite imagery, Teferi et al. (2011) found a noticeable increase (about 15 %) in the wetland vegetation areas over the Sudd region within the period from 1999 to 2006. A study by Awadalla (2011) found that the Sudd wetland average area is 50,000 km^2, while Dumont (2009) used multitemporal and multisensor remote sensing to estimate that the area of the Sudd swamp ranges from approximately 7,000 km^2 of permanent swamps to 90,000 km^2 of seasonal floodplain, while the total catchment area of the Sudd is nearly 3,000,000 km^2. Early studies at MIT showed a large area of swamp for the Bahar El Ghazal (Shamseddin et al. 2006), while Gaudet and Eagleson (1984) estimated the permanent swamp to be about 40,000 km^2. In addition, the Sudd wetland does not depend only on the local rainfall, but also on the inflow coming from Lake Victoria, and Tate et al. (2009) found a potential increase in lake levels in future scenarios which would contribute to increase the swamp area.

Some early studies have investigated the water balance for the three sub-basins (Mohamed et al. 2004; Sutcliffe et al. 1999; Hurst and Phillips 1938; Butcher 1938). The actual evaporation and soil moisture for wetlands in southern Sudan have also been examined by Mohamed et al. (2004) and Sutcliffe et al. (1999), who linked the swamps occurrence not only with the rainy season but also with fluctuations in the flow from Lake Victoria. The seasonal occurrence of the swamps in southern Sudan allows the

growth of different types of grasses (Green and El-Moghraby 2009) as well as the existence of several types of animals including the hippopotamus, antelopes, and fish. This highlights the importance of such land use/cover types for the ecosystems of the region.

Despite the importance of this swamp environment, only few previous studies examined the relationship between swamp and regional climate. Eltahir (1989) used a mathematical model to investigate soil–precipitation feedback mechanisms in annual rainfall over central Sudan, while Mohamed et al. (2005b) used a regional climate model to study the impact of the Sudd wetland on the Nile basin.

To date, an attempt to study the feedbacks of the swamp on the regional climate of southern Sudan, along with remote connections with East and West Africa climates, has not yet been conducted. In fact, this swamp region is located downstream of the Ethiopian Highlands, where most of the African easterly waves (AEWs) are triggered by local heating perturbations (Thorncroft et al. 2008; Leroux and Hall 2009; Sylla et al. 2011). These disturbances are recognized as the main mechanism in organizing rainfall patterns (e.g., Diedhiou et al. 1999) and therefore as key drivers of climate variability in Africa north of the equator. The AEWs occur mostly along a zonal circulation pattern, the so-called African easterly jet (AEJ) stretched from East to West Africa, which is driven by low level baroclinicity due to strong temperature and soil moisture gradients (Cook 1999; Thorncroft and Blackburn 1999; Steiner et al. 2009; Sylla et al. 2011). The location and strength of the AEJ strongly affect the amount of rainfall over the region (Mohr and Thorncroft 2006; Sylla et al. 2010a). The area of the swamps is located at the genesis region of the African easterly waves and at the entrance of the African easterly jet. Therefore, with a change in land cover over this region of East Africa, we can expect an impact on the climate of the region.

Here, we use the Abdus Salam International Centre for Theoretical Physics (ICTP) Regional Climate Model Version 3, RegCM3, to study the effects of the Sudd swamps of southern Sudan on the climate of the surrounding regions. We address this issue by intercomparing a series of sensitivity experiments in which the swamp area is substituted by bare desert soil. Hence, we first identify the swamp region over which the model employs a corresponding swamp land surface type in the "reference" experiment. We then replace this swamp land cover type by bare desert soil and analyze the effects of this change by comparison with the reference experiment. We stress that, in view of the abovementioned uncertainties in the quantification of the swamp area, we here use an idealized representation of the swamp, and therefore, our simulations should be mostly viewed as sensitivity experiments aimed at identifying first order effects of the swamp. Before discussing the results of this intercomparison (Section 5), in Sections 2 and 3, we first describe the model and experimental design, respectively, and in Section 4, we present a validation analysis of the model performance.

2 Model description and boundary forcing

As mentioned, in this study we use RegCM3, the third version of the ICTP regional climate model (Giorgi et al. 1993; Pal et al. 2007). This is a primitive equation, sigma vertical coordinate, limited area model based on the hydrostatic version of the dynamical core of the NCAR/PSU's mesoscale meteorological model MM5 (Grell et al. 1994). Radiative transfer is represented by the parameterization of Kiehl et al. (1996), and the description of planetary boundary layer processes is based on the scheme by Holtslag et al. (1990) in the implementation of Giorgi et al. (1993), while the scheme of Zeng et al. (1998) is used to represent fluxes from ocean surfaces. In RegCM3, convective precipitation can be described by a number of schemes, and based on some preliminary tests, we here use that of Grell et al. (1994) with the closure assumption of Fritsch and Chappell (1980). Resolvable scale precipitation processes are treated using the subgrid explicit moisture scheme (SUBEX) of Pal et al. (2000), which is a physically based parameterization including subgrid scale clouds, cloud water accretion, and evaporation of falling raindrops.

Of particular interest for this paper is the representation of land surface and hydrology processes. In RegCM3, these are represented by the biosphere–atmosphere transfer scheme (BATS, Dickinson et al. 1993), which includes a vegetation layer (with calculation of evapotranspiration, leaf drip, and leaf temperature), a soil model, and surface hydrology calculations. The soil zone in BATS has a depth of 3 m, divided into a 0.1-m surface layer, a vegetation-dependent root zone ranging from 1 to 2 m as a function

of vegetation type, and a 3-m deep soil layer. Soil moisture calculations include diffusion, gravitational drainage, and capillary processes, while surface runoff depends on the soil moisture content relative to saturation and the precipitation rate. Soil temperatures are calculated through a force restore method that captures the diurnal and seasonal temperature cycles. BATS can describe 20 different land surface types, each characterized by different properties, such as the Leaf Area Index, fractional vegetation cover, root density, soil texture and color, etc. (Dickinson et al. 1993). In particular, for swamp areas (type bog/marsh in BATS), the soil is constantly held at the saturation level (Table 1).

The initial and lateral boundary conditions for the RegCM3 simulations are obtained from the ERA Interim $1.5° \times 1.5°$ gridded reanalysis (Uppala et al. 2008), which is the third generation ECMWF reanalysis product. Sea surface temperatures (SSTs) used to force RegCM3 are obtained from the National Oceanic and Atmospheric Administration (NOAA) Optimum Interpolation (OI) SST dataset (Reynolds et al. 2007).

3 Experiment design

The regional model is integrated over Africa north of 10 °S and surrounding oceans as shown in the domain of Fig. 1, with a horizontal grid spacing of 30 km. The integrations start on May 1 until the end of August, with the month of May discarded from the analysis as spin up period. Each June–July–August (JJA) for the 10-year period 1990–1999 is

Table 1 Vegetation/land cover types (Dickinson et al. 1993)

1	Crop/mixed farming
2	Short grass
3	Evergreen needleleaf tree
4	Deciduous needleleaf tree
5	Deciduous broadleaf tree
6	Evergreen broadleaf tree
7	Tall grass
8	Desert
9	Tundra
10	Irrigated crop
11	Semi-desert
12	Ice cap/glacier
13	Bog and marsh
14	Inland water
15	Ocean
16	Evergreen shrub
17	Deciduous shrub
18	Mixed woodland
19	Forest/field mosaic
20	Water and land mixture

simulated and the climatology for the ten JJA simulation ensemble is analyzed. We selected the summer period because this is the main rainy season over the northern hemisphere tropical Africa. Although our simulations do not include the full seasonal cycle, most of the large-scale features considered in this study such as the African easterly jet, African easterly waves, and tropical easterly jet occur in the summer and are thus captured. Note that the domain exhibits some localized highlands around Cameroon (Cameroon Mountains), Central Nigeria (Jos Plateau), Guinea (Guinea Highlands), Ethiopia (Ethiopian Plateau), and West Sudan (Darfur high land), and a sharp gradient in variation of land cover is found from the Sahara Desert in the north to the dense forest in the south.

Three sets of experiments were undertaken. In the first (control simulation, or CTL), the land surface conditions are set to the default BATS parameters. These are obtained from the land cover dataset produced by the US Geological Survey Global Land Cover Characterization. In this dataset, the swamp region is somewhat underestimated compared to published estimates, so that in the first sensitivity experiment (called swampy), we extend the area of the swamp to make it closer to the maximum estimates. In the third experiment, the entire swamp area is replace by bare desert soil, so that comparison of the desert vs. swampy experiments provides an upper estimate of the effects of the swamp. We stress again that our simulations should be considered as simple sensitivity experiments aimed at assessing first order effects, consistent with the uncertainties in the model representation of land surface processes and in the accurate quantification of the swamp area. The land surface map of the control case is shown in Fig. 2a, while that of the sensitivity experiments is in Fig. 2b. The BATS parameters for the swamp and desert soil land surface types are reported in Table 2. Note that in the case of swamp, the land surface is kept continuously at the saturation level, so that it provides a strong moisture

source to the atmosphere and does not consider the sources of the swamp explicitly. Over other areas, BATS initializes soil moisture by prescribing the soil water content relative to saturation as a function of land cover type (Giorgi and Bates 1989).

Simulated precipitation is validated against two observational datasets: GPCP (2.5°×2.5° resolution; Adler et al. 2003) and Climate Research Unit (CRU, land only, 0.5°× 0.5° resolution; Mitchell et al. 2004). GPCP is a satellite–gauge-merged rainfall product, while CRU is a purely gridded gauge dataset, and thus, they can be quite different over some areas. In fact, Sylla et al. (2012) extensively analyzed different gridded observed rainfall products and found that they do exhibit substantial systematic differences in the mean precipitation amounts, with GPCP showing generally larger amounts than CRU over West and East Africa. It is difficult to unambiguously assess which is the best dataset, since they are based on different data and processing. Therefore, the use of multiple datasets in the comparison is required to provide an estimate of related uncertainties.

Surface air temperature is validated against CRU data, while the atmospheric circulation, relative humidity, and total cloud cover in the interior domain are compared to the ERA Interim data used to drive the model at the lateral boundaries. Outgoing longwave radiation is validated against NCAR archives, with gaps filled with temporal and spatial interpolation (Liebmann and Smith 1996).

4 Model validation

4.1 Rainfall climatology

In this section, we first validate the spatial patterns of seasonal precipitation. Figure 3 compares averaged JJA

Fig. 2 The land cover map for the swamp region: **a** the control, **b** the swamp. The category for each land cover is shown in Table 1
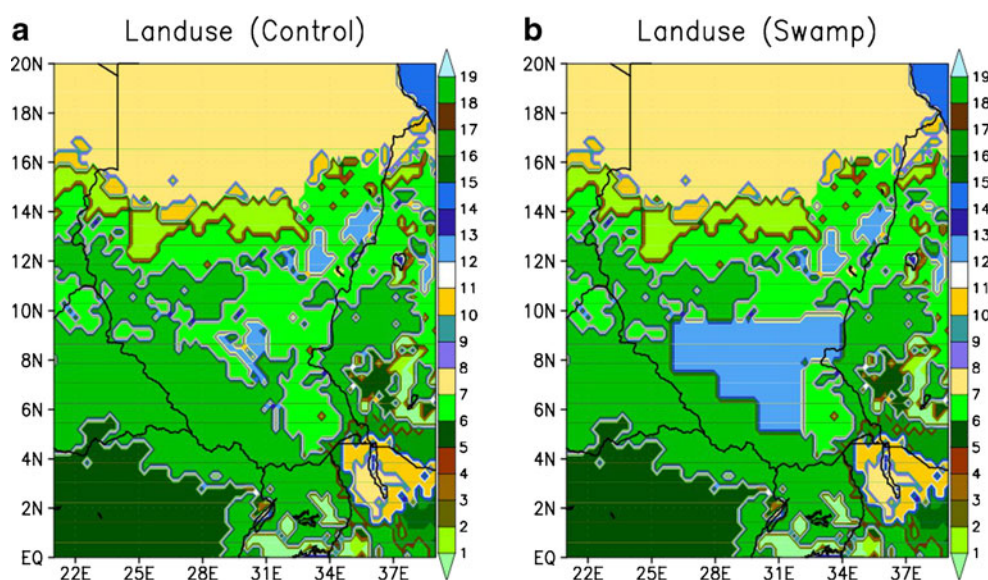
Table 2 Vegetation/land cover parameters for bare desert soil and swamp

Parameter	Bare desert soil	Swamp
Maximum fractional vegetation cover	0	0.8
Difference between maximum fractional vegetation cover and cover at temperature of 269 K	0	0.4
Roughness length (m)	0.05	0.03
Depth of the rooting zone soil layer (m)	1	1
Depth of the upper soil layer (m)	0.1	0.1
Fraction of water extracted by upper layer roots (saturated)	0.9	0.5
Vegetation albedo for wavelengths >0.7 μm	0.2	0.06
Vegetation albedo for wavelengths >0.7 μm	0.4	0.18
Minimum stomatal resistance (s m^{-1})	200	200
Maximum LAI	0	6
Minimum LAI	0	0.5
Stem (and dead matter area index)	0.5	2
Inverse square root of leaf dimension (m$^{-0.5}$)	5	5
Light sensitivity factor (m^{2}W^{-1})	0.02	0.02

GPCP and CRU precipitation (Fig. 3a, b) with the corresponding RegCM3 field (Fig. 3c). Also shown are the differences between the RegCM3 field and the two observational datasets (Fig. 4a, b). In JJA, the ITCZ approaches its northernmost location. Therefore, observed precipitation (CRU and GPCP) (Fig. 3a, b) over the continent is mostly confined between 5°S and 18°N, while regions above and below these latitudes are predominantly dry. This pattern of precipitation is mainly associated to the occurrence of propagating the mesoscale convective system related to the dynamics of AEJ, AEW, and Tropical Easterly Jet (TEJ) (d'Amato and Lebel 1998; Jenkins et al. 2005). The CRU data exhibit three precipitation maxima around the Guinea Highlands, Cameroon Mountains, and Ethiopian Highlands which are associated with local orographic features (see Fig. 1), while GPCP shows less rainfall over the Ethiopian Highlands, probably because of its coarse resolution.

The model captures the general patterns of the observed rainfall distribution, in particular the ITCZ position, intensity, and break over West Africa as well as the orographic rainfall in the complex terrains of Ethiopian Highlands, Guinea Highlands, and Cameroon Highlands. However, precipitation over southern Sudan and the Ethiopian Highlands is overestimated due to the orographic effect and the high convergence over this region. Also, the monsoon rain belt appears narrower in the model than in the two observation datasets, and precipitation over the Atlantic branch of the ITCZ is underestimated.

Table 3 displays the precipitation bias (in mm/day and in %) over the three East Africa subregions shown in Fig. 1 compared to the CRU and GPCP climatologies. The model overestimates precipitation over all regions. The biases are in the range of about 9 to 37 %, with the values being largest over central Sudan and the Ethiopian Highlands and generally higher compared to the CRU data than the GPCP ones.

It should be noted that considerable differences exist across the observed precipitation climatologies (Sylla et al. 2012), so that our RegCM3 simulation appears reasonable given this uncertainty. We also note that the performance of our model version appears in line with previous works performed using either the RegCM system in various configurations (Sun et al. 1999; Pal et al. 2007; Anyah and Semazzi 2007; Sylla et al. 2010b; Steiner et al. 2009) or other regional modeling systems (e.g., Vizy and Cook 2002; Nikulin et al. 2012; Paeth et al. 2005; Gallée et al. 2004; Flaounas et al. 2010; Druyan et al. 2008).
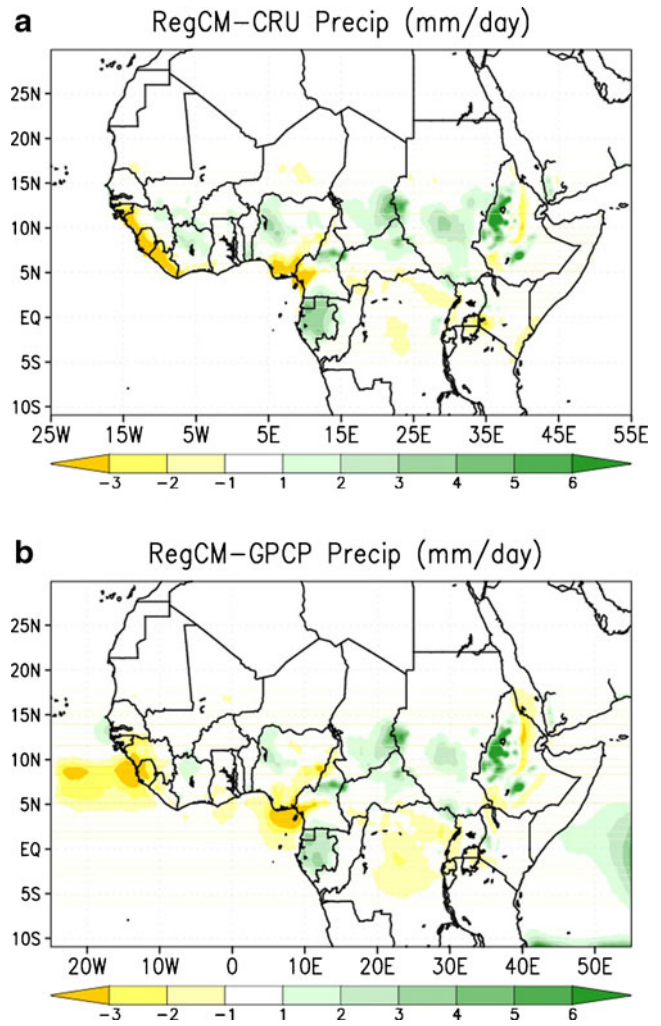
4.2 Temperature climatology

The seasonal average of JJA 2-m temperature for 1990 to 1999 is illustrated in Fig. 5. The figure presents CRU observations (Fig. 5a), RegCM3-simulated values (Fig. 5b), and the difference between CRU and RegCM3 (Fig. 5c) temperatures. In JJA (Fig. 5a), the CRU observations place the lowest temperatures mostly over the mountainous areas of West and East Africa and the Greater Horn of Africa. The warmest areas are confined between 15 °N and 27 °N with larger values located over the Sahara desert. RegCM3 (Fig. 5b) reproduces well this spatial pattern but it shows a systematic cold bias of a few degrees in the convective regions south of 15 °N (Fig. 5c).

This cold bias over tropical and equatorial Africa has been a persistent feature in RegCM3, as also found for example in the experiments of Sylla et al. (2010b), although the magnitude of the bias is somewhat reduced in our
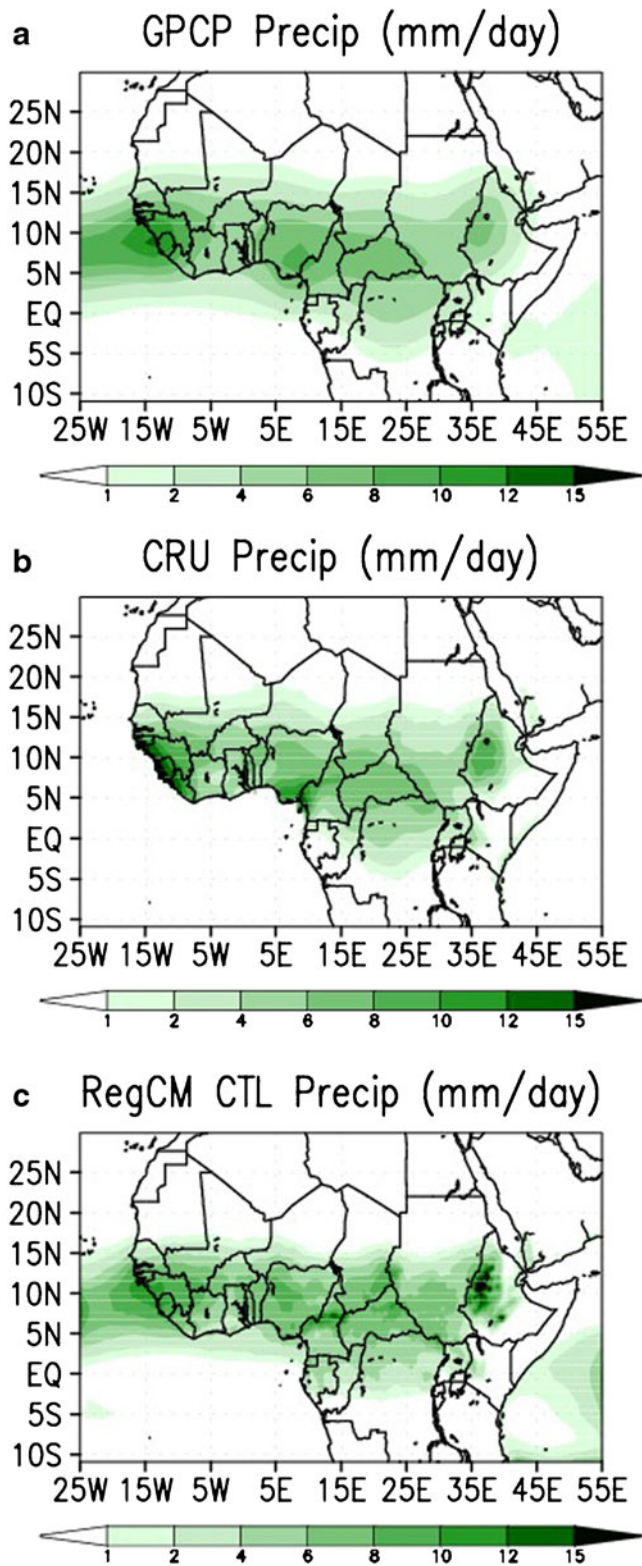
Fig. 3 Averaged precipitation (in mm/day) for JJA 1990–1999: **a** GPCP, **b** CRU, **c** RegCM
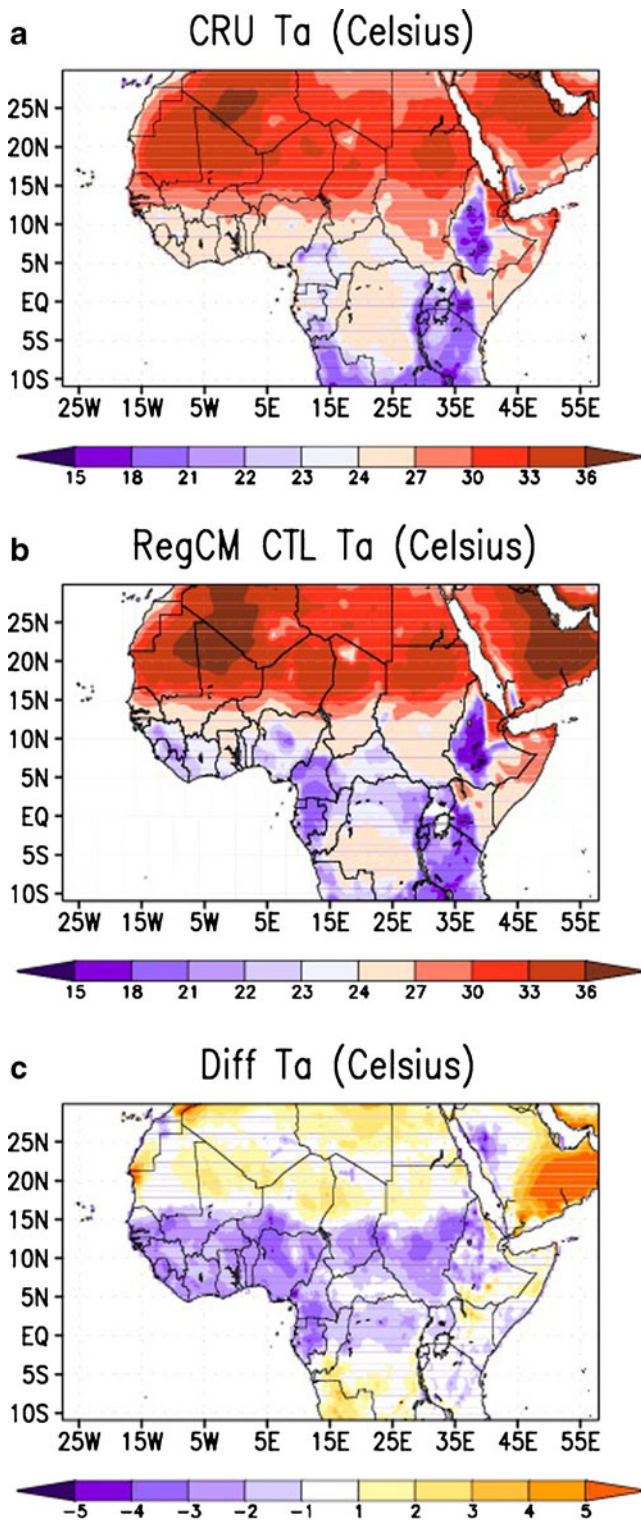

Fig. 4 Averaged precipitation bias (in mm/day) for JJA 1990–1999: **a** RegCM-CRU, **b** RegCM-GPCP

in remote areas (Mitchell et al. 2004). In addition, surface temperature depends on many parameters, such as albedo, evapotranspiration rates, location and height of the observing gauges, etc., which are also highly uncertain, and on the

Table 3 The precipitation bias (in mm/day and in %) and the root mean square error (RMSE) over the three East African subregions shown in Fig. 1

Subregion	Control					
	Bias		RMSE		Bias %	
	CRU	GPCP	CRU	GPCP	CRU	GPCP
South Sudan	0.84	0.57	0.60	0.08	16.04	8.75
Central Sudan	1.24	0.5	0.85	0.12	37.90	20.63
Ethiopian Highlands	2.07	2.11	1.79	0.29	26.64	26.52

simulation. It should be stressed that the CRU observations are possibly affected by large uncertainties in this region due to the relative sparseness of observing stations, particularly
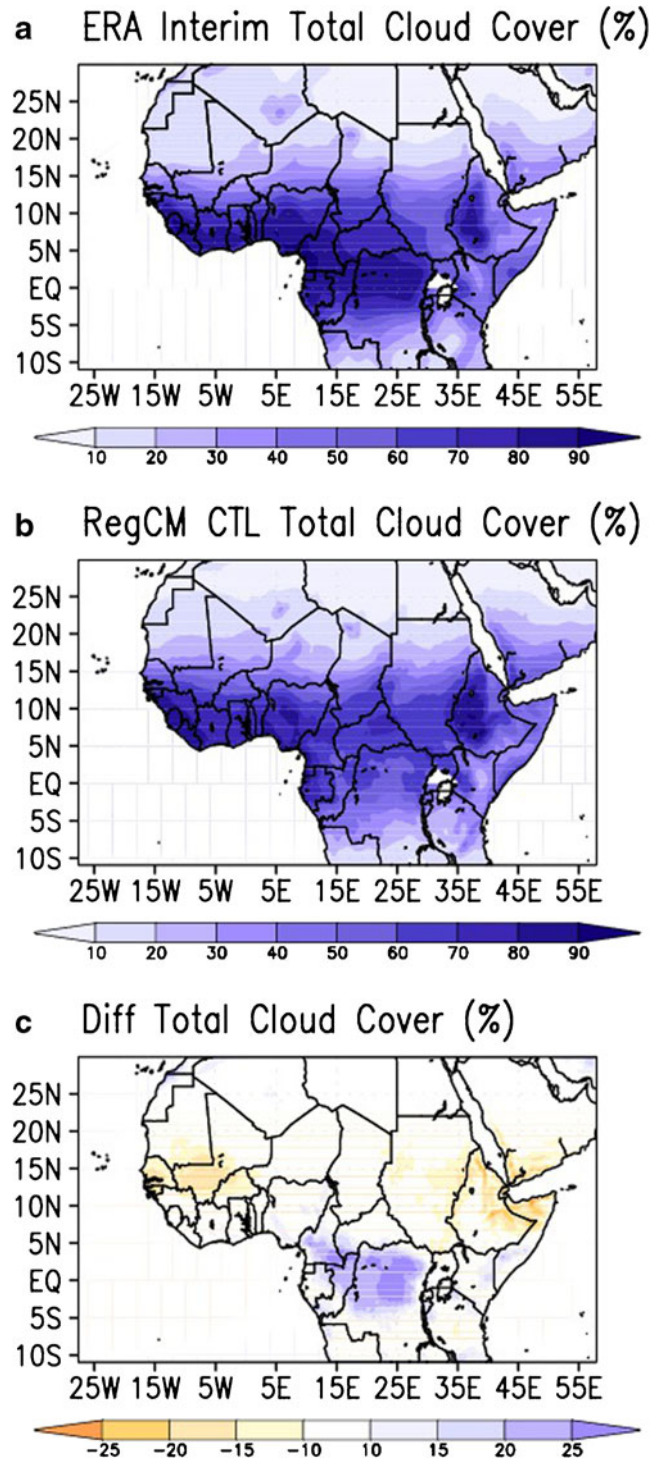
Fig. 5 Averaged 2-m air temperature (in °C) for JJA 1990–1999: **a** CRU, **b** RegCM, **c** RegCM minus CRU difference

4.3 Total cloud cover climatology and outgoing longwave radiation

In this section, the spatial pattern of seasonal (JJA) total cloud cover (TCC) and OLR are validated. Figure 6 shows the averaged JJA ERA Interim TCC (Fig. 6a) and the

Fig. 6 Averaged total cloud cover (in %) for JJA 1990–1999: **a** ERA Interim, **b** RegCM, **c** ERA Interim minus RegCM

presence of dust and aerosols. Given all these uncertainties, we assess that a model bias of a few degrees is acceptable for a sensitivity experiment such as in this paper.

corresponding RegCM3 field (Fig. 6b) along with their difference (Fig. 6c). We note that the total cloud cover is calculated using the random overlapping method. In good agreement with the rainfall distribution, the regional model captures the general pattern of the observed TCC, in particular the maxima over the Ethiopian and Gulf of Guinea Highlands and the minima over the Sahara Desert and south of the equator. However, compared to ERA Interim, the model underestimates could cover over the Congo basin and overestimates it along the Western Sahel band and the Horn of Africa.

The OLR is validated against observations from the abovementioned NOAA dataset. Figure 7 shows the averaged JJA NOAA OLR (Fig. 7a) and the corresponding RegCM3 field (Fig. 7b) along with their difference (Fig. 7c). The spatial distribution of OLR is in good agreement with that of the TCC previously discussed. Both the model and the observations (Fig. 7a, b) exhibit larger (lower) OLR values in North Africa and south of 5 °S (along the ITCZ) because of smaller (larger) amount of cloud cover. Consistent with the TCC results, simulated OLR is underestimated over the Congo basin due to an overestimation of TCC. Nevertheless, the model manages to capture generally well the general features of the OLR pattern in both magnitude and spatial extent.

4.4 Climatology of dynamical features

4.4.1 Low level circulation

The spatial patterns of average JJA low level (925 mb) circulation and relative humidity (RH) are shown in Fig. 8a for the ERA Interim reanalysis and Fig. 8b for the RegCM3 simulation. Direct observations of relative humidity over the region are not available, and thus, we use here the driving reanalysis (which is the closest information to reality that we have available) for model validation. Overall, the model reproduces well the main features of the low level circulation, such as the low level monsoon flow over West Africa, the northerly Harmattan flow over East Africa, and the southeasterly flow over the Horn of Africa. The relative humidity field, with relatively high values in the ITCZ between 5 °S and 15 °N is also well captured, although the RH values are somewhat lower than in the reanalysis over areas of central equatorial Africa. Overall, Fig. 8 indicates that RegCM3 exhibits a good performance in the simulation of the low level circulation over the selected domain.

4.4.2 Tropical easterly jet

The TEJ develops between 200 and 150 mb in the upper troposphere over India in response to a large
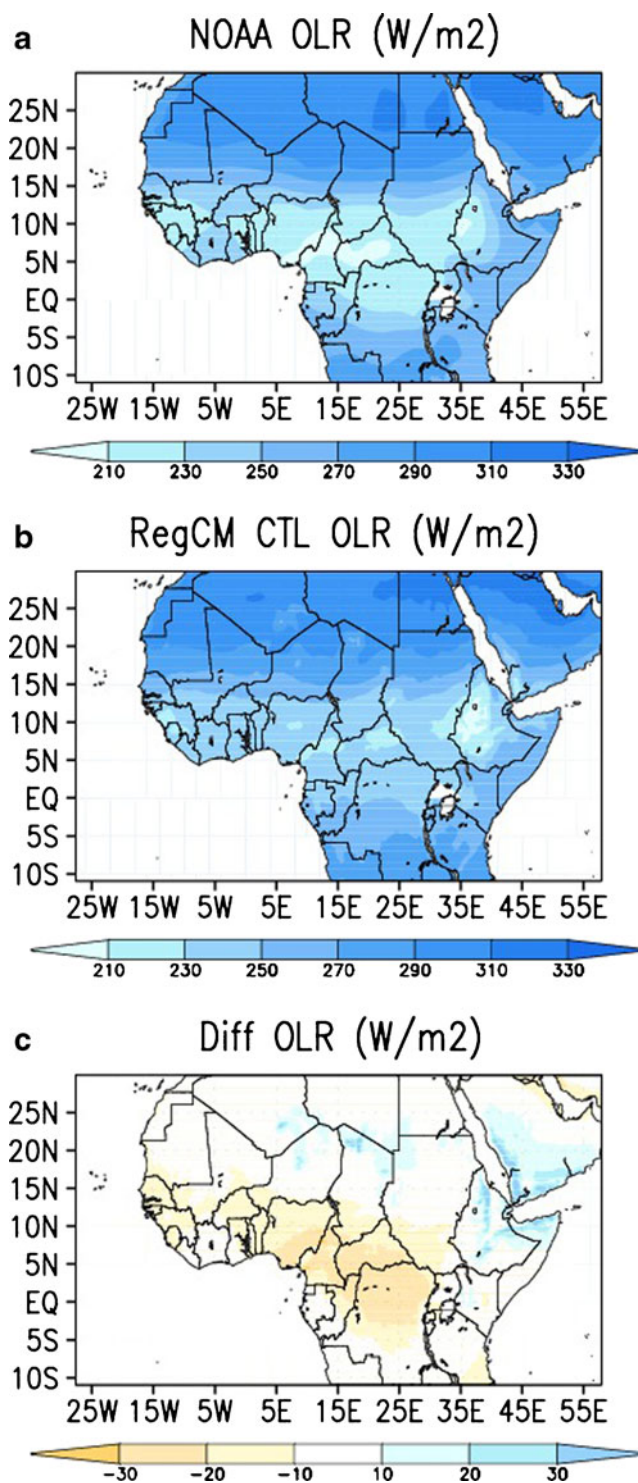
Fig. 7 Averaged outgoing longwave radiation (in W/m²) for JJA 1990–1999: **a** NOAA, **b** RegCM, **c** NOAA minus RegCM

meridional thermal gradient and settles during the northern summer Asian monsoon season between the Tibetan Highlands and the Indian Ocean (Fontaine and Janicot 1992; Koteswaram 1958; Chen and van Loon 1987). It stretches from the Indochina peninsula, across the
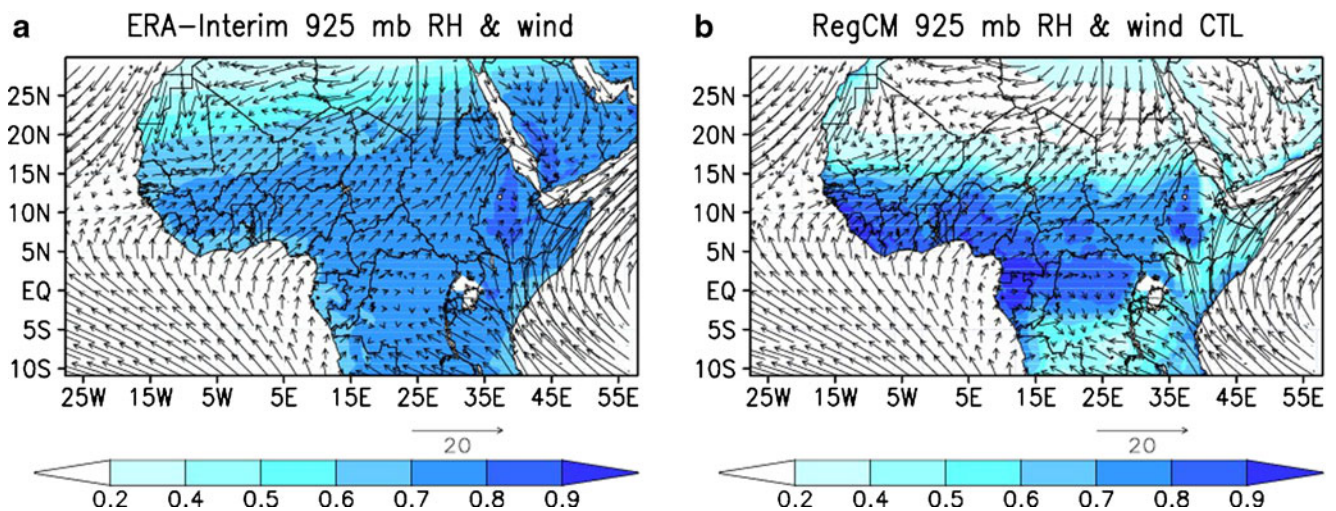
Fig. 8 The *blue colors* show the averaged relative humidity for JJA 1990–1999, and the *black arrows* which were superimposed at 925 mb represent the wind vector: **a** ERA Interim, **b** RegCM

African continent, to the tropical Atlantic (Wu et al. 2009), and it is linked to anomalous SSTs on a planetary scale (Chen and van Loon 1987). The TEJ is one of the planetary features that contribute to the northern African summer climate variability (Chen and van Loon 1987). Figure 9a shows the TEJ in the ERA Interim reanalysis confined between 3 °N and 17 °N with a core speed exceeding 20 m/s. The band of the jet decreases gradually from East Africa to West Africa. In fact, the highest wind speed of about 25 m/s occurs over the Horn of Africa and the western Indian Ocean, while the lowest values of about 11 m/s are found over Senegal.

RegCM3 in Fig. 9b reproduces well the structure of the TEJ shown in the ERA Interim reanalysis. It captures both the location and intensity of the jet. However, it extends the core of the jet with winds of about 20 m/s further to the north in the Central African Republic and southern Chad. In addition, it extends also the 16-m/s zone further across Nigeria, Benin, and Togo.

4.4.3 African easterly jet

The AEJ results mainly from the vertical inversion (around 600–700 mb) of the meridional thermal gradient between the Sahara and equatorial Africa due to the existence of strong surface baroclinicity (Cook 1999; Steiner et al. 2009) associated with atmospheric deep convection (Thorncroft and Blackburn 1999; Sylla et al. 2010b). Figure 9c shows the ERA Interim zonal wind in JJA at 600 mb. It is confined approximately between 7° N and 23 °N extending from Chad to the Atlantic Ocean with a core speed ranging from 11 to 13 m/s located over West Africa. As for the TEJ, RegCM3

simulates reasonably well both the strength and location of the jet (Fig. 9d).

4.4.4 African easterly waves

AEWs are crucial synoptic features of the summer climate of West Africa and the tropical Atlantic. The initiation of these waves around Darfur and the Ethiopian Highlands and their subsequent development over West Africa and the Atlantic coast are associated with convection and latent heat release (Thorncroft et al. 2008; Leroux and Hall 2009; Sylla et al. 2011). They are key drivers of climate variability as they contribute to organizing rainfall patterns in this region (Diedhiou et al. 1999).

Figure 9e, f illustrates the AEWs activity in the summer season (JJA) from 1990 to 1999 from ERA Interim and RegCM3, respectively. In the figure, the AEW activity is measured by the 3–5-day bandpass-filtered 600-hPa meridional wind variance averaged over the whole simulation period (Mekonnen et al. 2006). The largest wave activity is located over West Africa and the adjacent Atlantic Ocean. Compared to the ERA Interim reanalysis, the regional climate model captures these maxima over West Africa and the Atlantic Ocean but shows some underestimation over East Africa. In fact, the tilted zonal band in which the high wave activity is embedded is stretched back to the Darfur and Ethiopian complex terrains where the AEWs are generated. However, compared to the study of Mekonnen et al. (2006) and Ruti and Dell'Aquila (2010), both using ERA40 reanalysis, the simulation appears to be of improved performance.

In summary, the relatively high resolution version of the RegCM3 used here shows a good performance in simulating
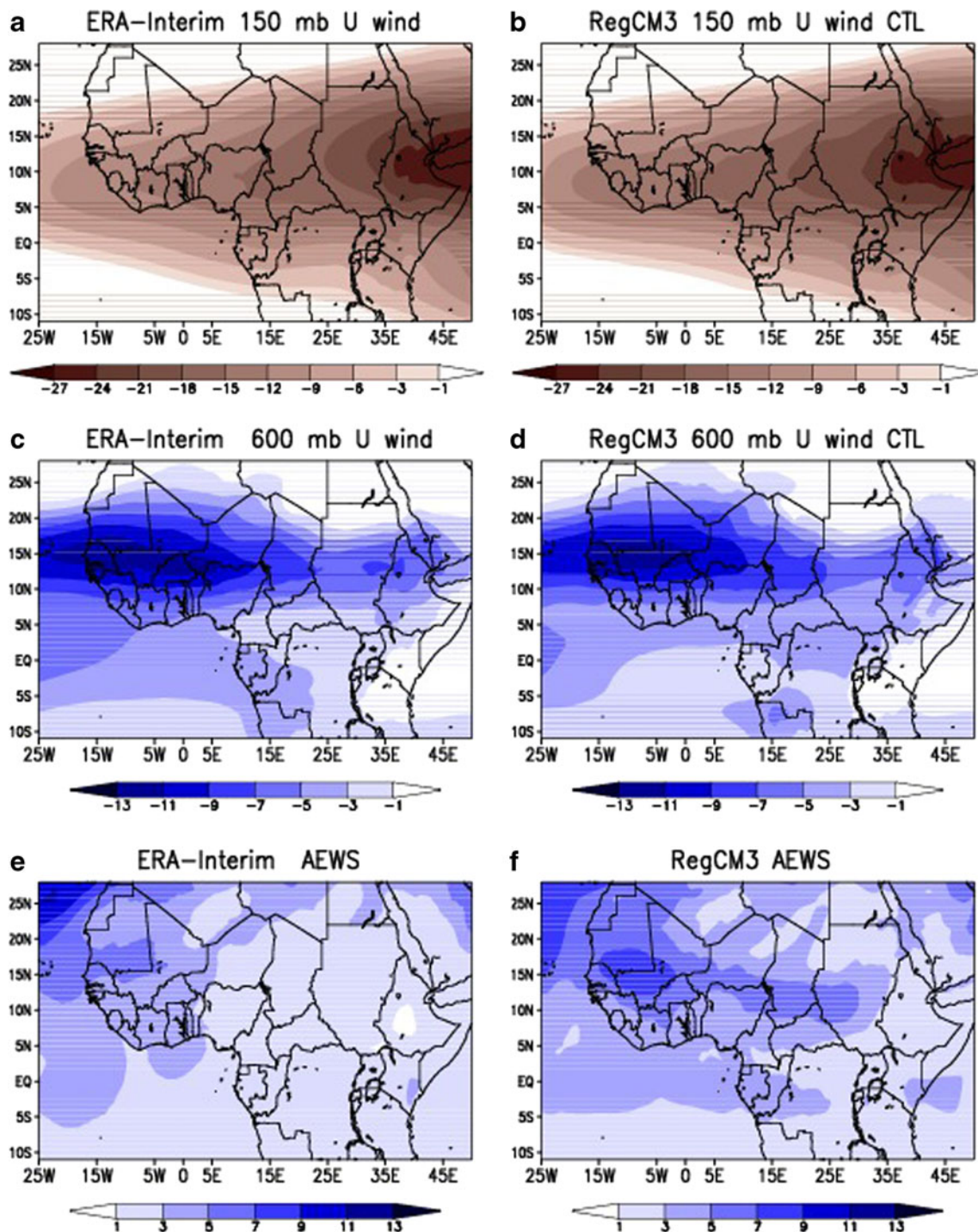
Fig. 9 Averaged zonal wind (in m/s) for JJA 1990–1999: **a** ERA Interim at 150 mb, **b** RegCM at 150 mb, **c** ERA Interim at 600 mb, **d** RegCM at 600 mb. The AEWs are shown in the lower panel for JJA 1990–1999: **e** ERA Interim, **f** RegCM

the climatology of rainfall over Africa north of the equator, along with the features that control the dynamic of the summer climate of the region, which is in line and in fact better in several instances, compared to previous coarser resolution versions of this model. In addition, previous studies have shown that this model is also able to capture reasonably well the variability of such features and the interaction between them and small-scale processes (Sylla et al. 2011; Sylla et al. 2010a). Therefore, although some biases persist, namely a tendency for overestimating precipitation and underestimating temperature, given the uncertainties in observations, we assess that the model is suitable to examine the first order local and remote effects of land cover changes on the African summer monsoon climate.

5 Impact of the land cover change

5.1 Impact on rainfall and ground temperature

The mean JJA ground temperature differences between the swamp and control simulations and between the swamp and bare desert soil case are shown in Fig. 10a, b. In the former case, the swamp produces a cooling of less than 1 °C, while in the latter, the cooling compared to desert conditions reaches locally 2 °C. A two-tailed Student's t test was carried out to estimate the statistical significance of the land use effects at the 95 % confidence level, i.e., that there is a 95 % probability that the change is not occurring by chance. In both cases, this local cooling is statistically significant at
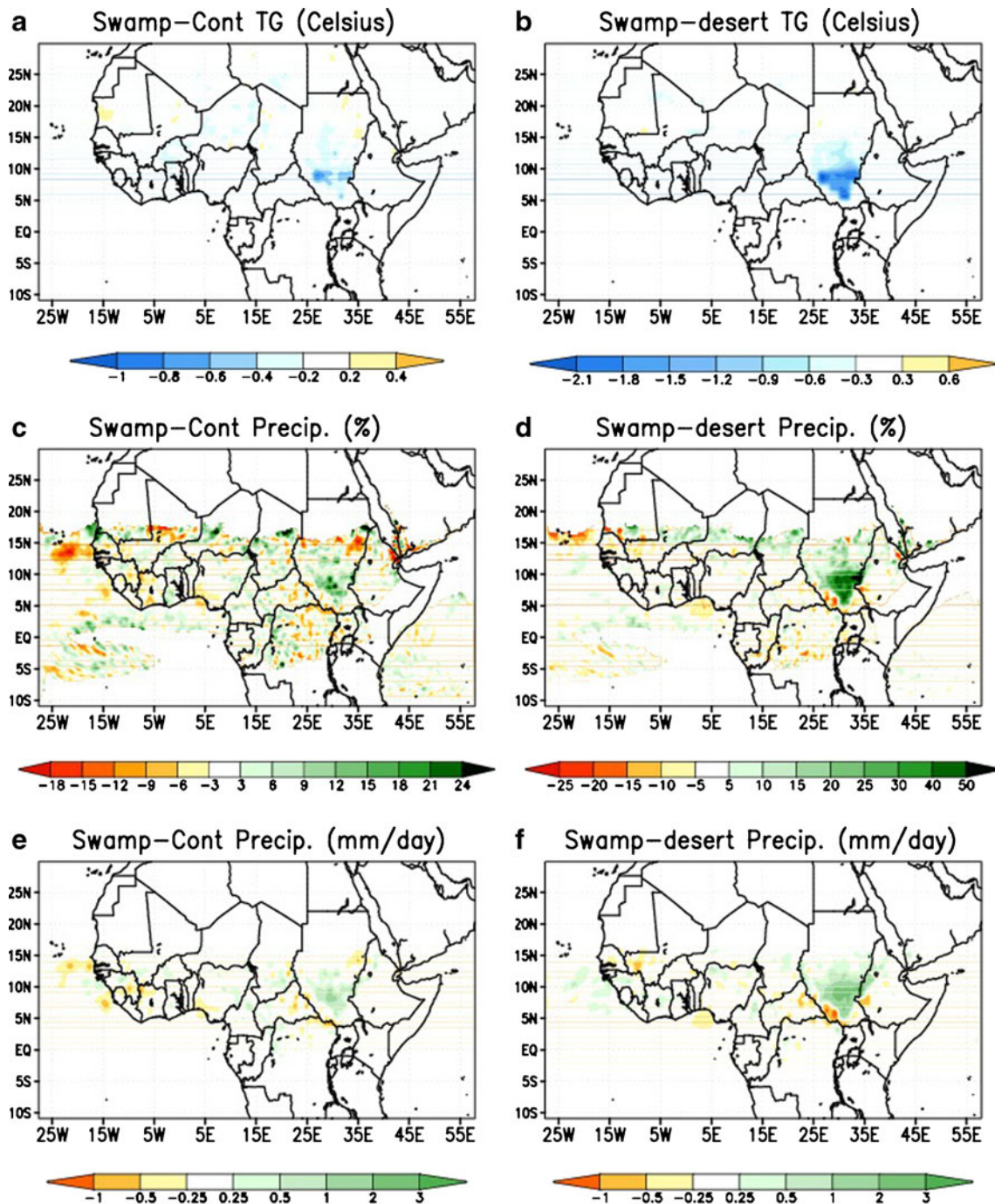
Fig. 10 The *upper panels* show the averaged ground temperature (in °C) for JJA 1990–1999: **a** swamp − control, **b** swamp − bare desert soil; the *middle panels* show the percentage of the precipitation for JJA 1990–1999: **c** swamp − control, **d** swamp − bare desert soil. The *lower panels* show the difference in precipitation for JJA 1990–1999: **e** swamp − control, **f** swamp − bare desert soil

the 95 % confidence level. Mohamed et al. (2005b) find increases in the screen level temperature by 4 to 6 °C during the dry season and 0.5 to 1 °C during the wet season when the swamp region is drained, a result in line with those found here. Figure 10a, b also shows that the cooling effect by the swamp is mostly localized in nature.

The rainfall differences between the swamp and control experiment and between the bare desert soil and control experiment are shown in c and d (in mm/day) and e and f of Fig. 10 (in % of control value), respectively. In both cases, the moisture source associated with the swamp increases rain locally by 9 to 21 % compared to the control simulation and by up to 40 % compared to the bare desert soil conditions. These precipitation effects over the swamp area are statistically significant at the 95 % confidence level.

Figure 11 shows the mean monthly precipitation along with the interannual standard deviation in the bare desert soil and swamp experiments over the three regions depicted in Fig. 1: southern Sudan, central Sudan, and Ethiopian Highlands. The largest effects are found over the southern

Fig. 11 The standard deviation and mean rainfall for JJA 1990–1999: **a** swamp and bare desert soil over southern Sudan, **b** swamp and bare desert soil over central Sudan, and **c** swamp and bare desert soil over Ethiopian Highlands
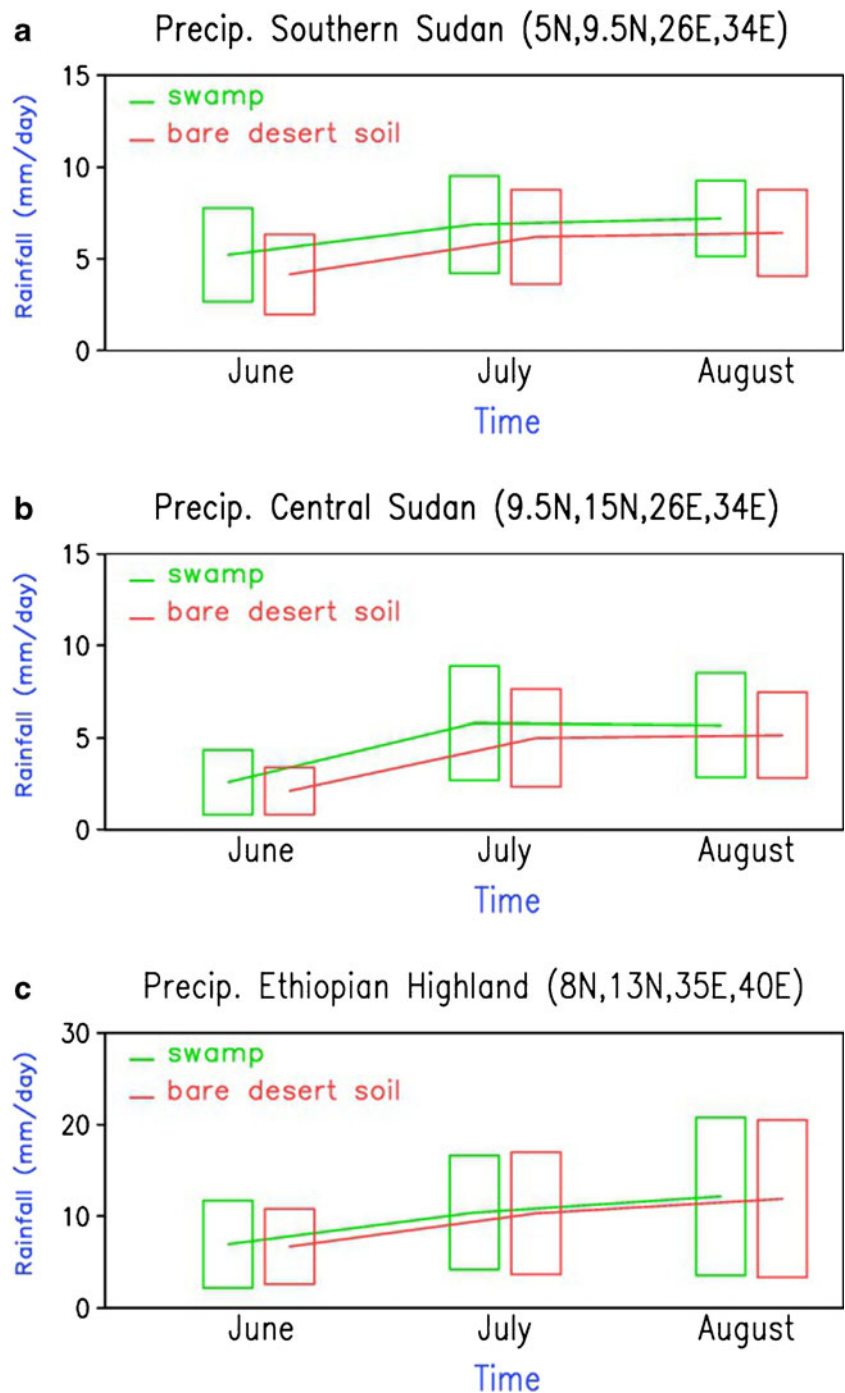
Sudan swamp region, while the smallest, almost negligible over the Ethiopian Highlands. In all cases, the increase in precipitation induced by the swamp is much lower than the interannual standard deviation and it does not alter the seasonal evolution of rainfall over the selected subregions.

It is interesting to note that these wetter conditions induced by the swamp are found not only across the swamp area, but also north of it in central Sudan and, especially for the swamp minus bare desert soil case, across the Sahel region far from the swamp, although we did not find this
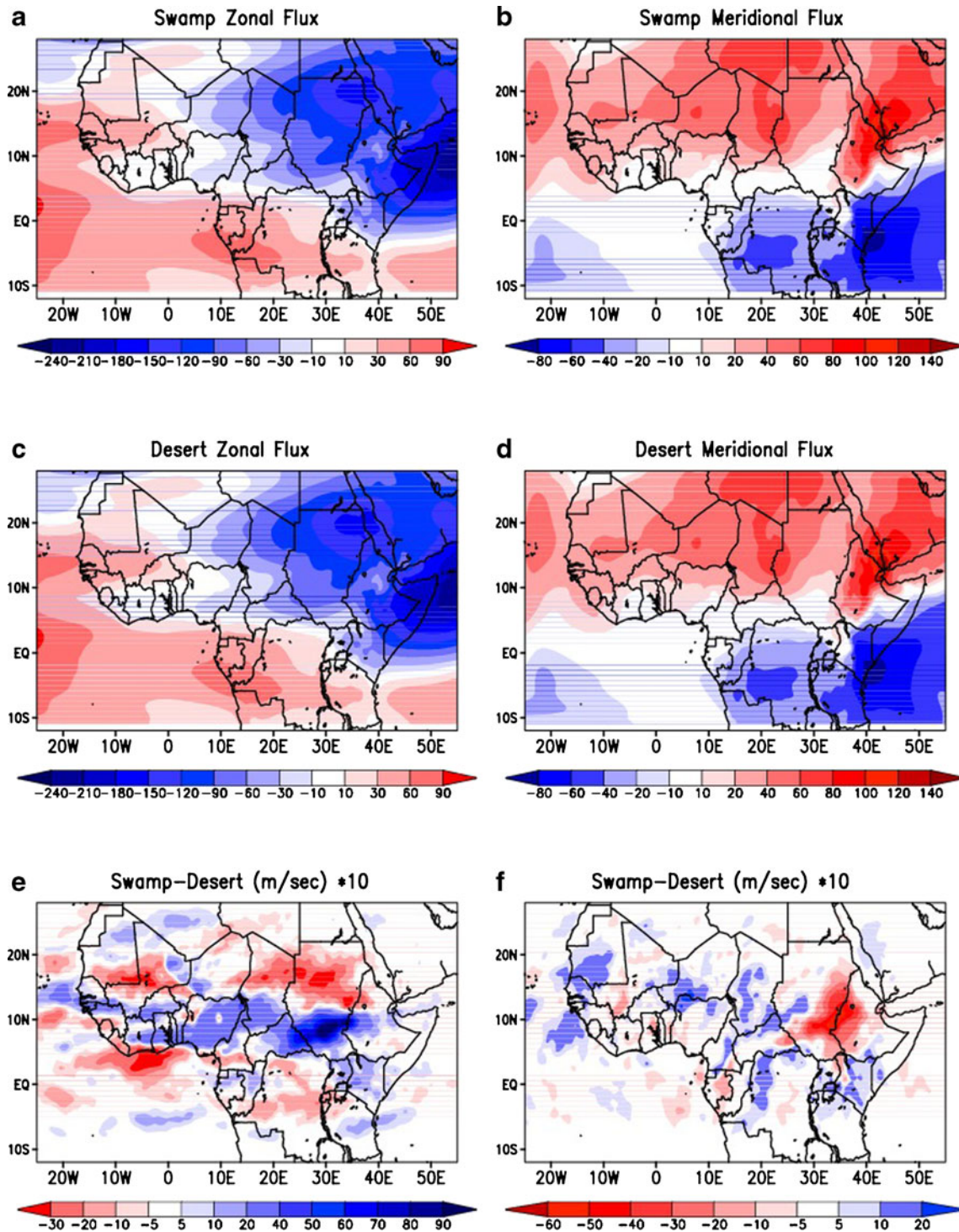
Fig. 12 Averaged zonal and meridional flux (in m/s) for JJA 1990–1999: **a** swamp zonal flux, **b** swamp meridional flux, **c** bare desert soil zonal flux, and **d** bare desert soil meridional flux. The differences are shown in the *lower panels* for JJA 1990–1999: **e** zonal swamp flux − zonal desert soil flux, **f** meridional swamp flux − meridional bare desert soil flux
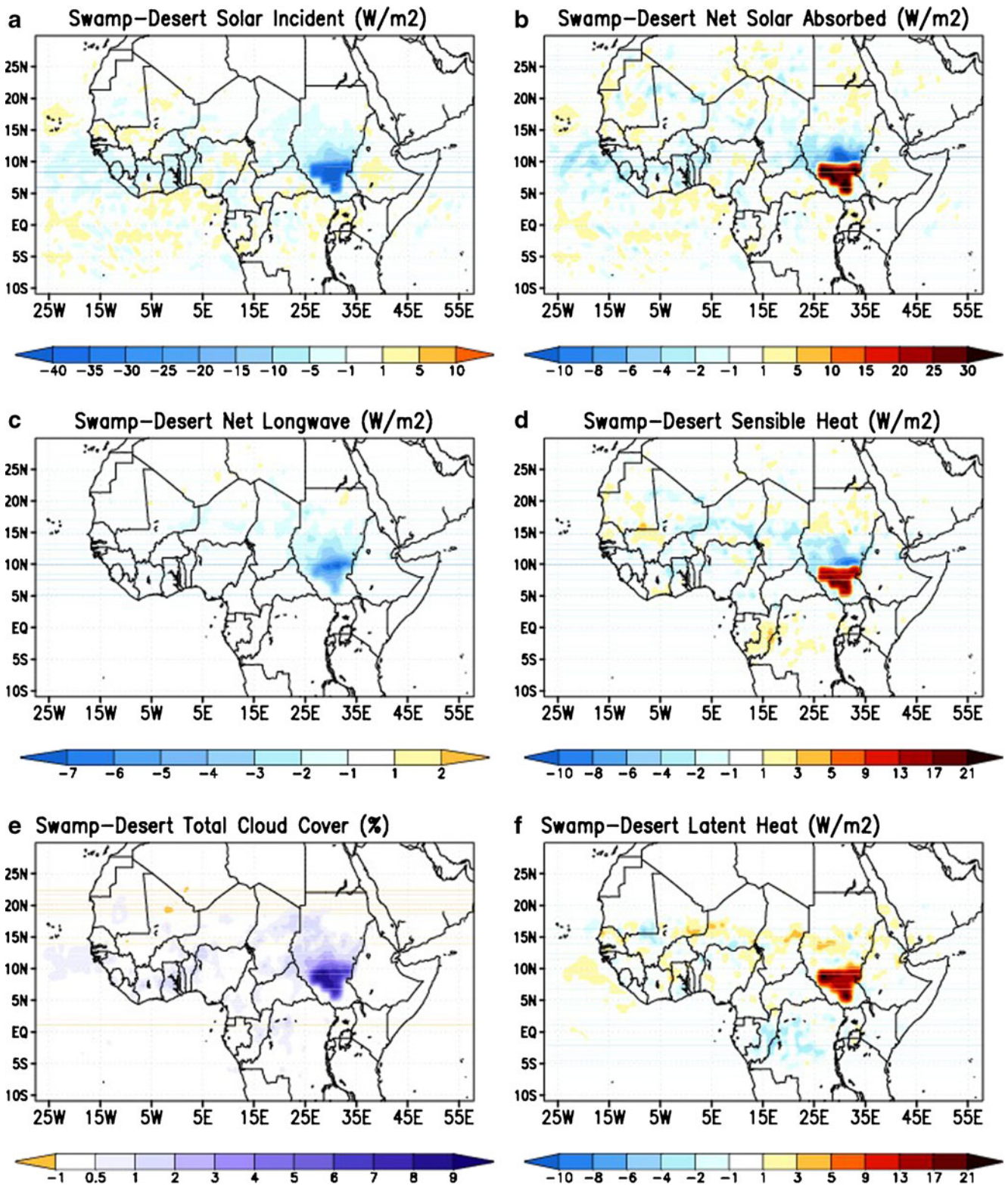
Fig. 13 The *upper panels* show the difference between the swamp and bare desert soil: **a** the averaged solar incident (in W/m²) for JJA 1990–1999 on the *left* and **b** the averaged net solar absorbed (in W/m²) for JJA 1990–1999 on the right. The *middle strips* show the difference between the swamp and bare desert soil: **c** the averaged net longwave (in W/m²) for JJA 1990–1999 on the *left* and **d** the sensible heat (in W/m²) for JJA 1990–1999 on the *right*. The *lower panels* show the difference between the swamp and bare desert soil: **e** the averaged total cloud cover for JJA 1990–1999 on the *left* and **f** the averaged latent heat (in W/m²) for JJA 1990–1999 on the *right*

Table 4 The difference in ground temperature and the radiation budget components between the swamp simulation and the bare desert soil simulation averaged over south Sudan and Central Sudan

Variable	Central Sudan (26 °E, 34 °E, 9.5 °N, 15 °N)	Southern Sudan (26 °E, 34 °E, 5 °N, 9.5 °N)
Ground temperature (tg), K	−0.6	−1.27
Sensible heat (sh), W/m^2	−3.1	9.5
Latent Heat (lh), W/m^2	1.5	10.8
Net longwave (lwn), W/m^2	−3.0	−2.4
Net solar absorbed (swn), W/m^2	−4.3	19.2
Downward longwave (lwd), W/m^2	0.52	3.4
Solar incident (swi), W/m^2	−7.7	−25.4

increase to be statistically significant at the 95 % confidence level. These changes may originate at first order from modifications in the moisture flux distribution.

Figure 12 presents the column integrated zonal and meridional moisture flux components for both sensitivity experiments along with their differences. Over East Africa, the zonal (Fig. 12a, c) and meridional (Fig. 12b, d) moisture fluxes are dominated by easterlies and southerlies, respectively. Both experiments exhibit similar spatial distribution but with different magnitudes. In fact, the swamp scenario produces a weaker meridional flux (Fig. 12f) in eastern Sudan adjacent to Ethiopian Highlands and a larger zonal flux (Fig. 12e) over southern Sudan in the swampy region, thereby favoring more rainfall locally. Other mechanisms associated with these local and remote effects are discussed below.

5.2 Impact on the surface radiation budget

The seasonal differences of some components of the surface energy budget (incident solar energy; net absorbed short-wave, net longwave, and sensible and latent heat fluxes) along with the changes in cloud cover averaged during JJA from 1990 to 1999 are displayed in Fig. 13. Figure 13a shows that, compared to the bare desert soil experiment, the swamp scenario decreases the shortwave radiation reaching the surface in both the southern and central Sudan regions because of higher cloud amounts (Fig. 13e). However, the net absorbed shortwave exhibits a dipole pattern with an increase in the south and a decrease to the north (Fig. 13b). The increase in absorbed solar energy mirrors the change in the land cover and therefore can be
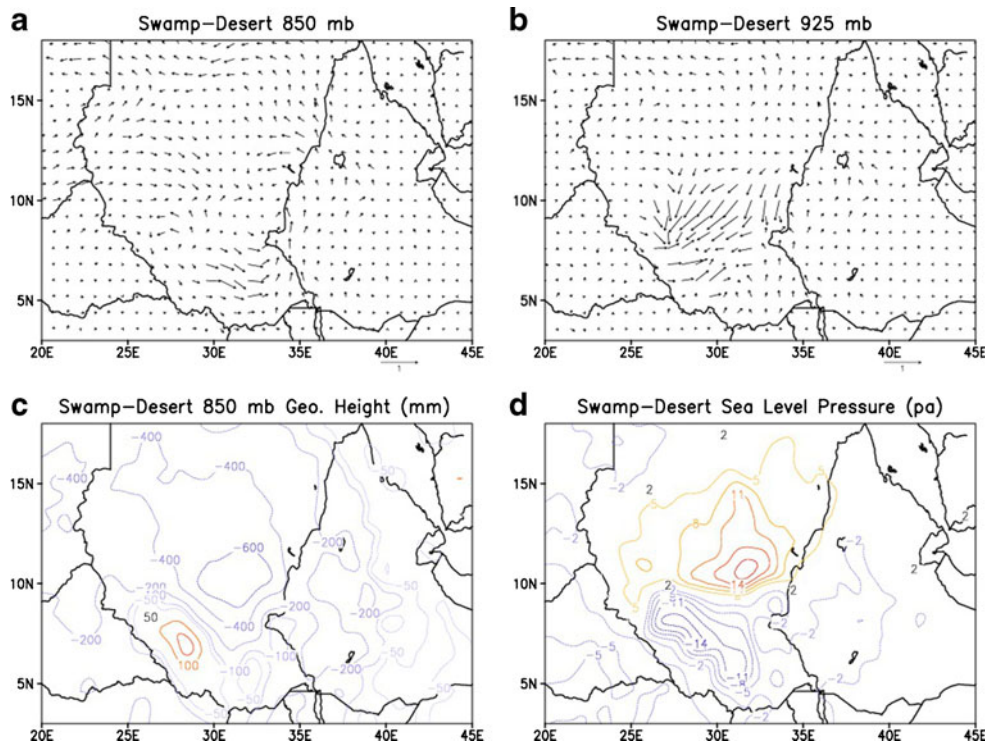
Fig. 14 The *upper panels* show the averaged vector low level wind for swamp minus bare desert soil for JJA 1990–1999: **a** at 850 mb, **b** at 925 mb. The *lower bands* show the average sea for JJA 1990–1999 for the swamp minus bare desert soil: **c** the geopotential height at 850 mb, **d** the sea level pressure (in Pa)

attributed to the lower albedo of the swamp. The net long-wave distribution (Fig. 13c) is lower in many parts of Sudan in the swamp experiment because of reduced surface temperatures (and thus reduced upward longwave flux) and increased cloudiness (and thus increased downward longwave flux). The sensible heat flux (Fig. 13d) difference shows a dipole pattern similar to that of the net absorbed shortwave radiation, whereas the latent heat (Fig. 13f) exhibits its maximum around the swamp region. Mohamed et al. (2005a) used two radiation stations, one in Kenya and one in Saudi Arabia to validate their model. However, the effect of the swamp on the entire radiation budget was not analyzed. We tried to fill this gap and examined the impact of the swamp on radiation parameters over the region. Table 4 summarizes the ground temperature, latent and sensible heat, and surface radiation budget component changes averaged over the regions identified in Fig. 1. In general, the turbulent heat flux changes help to balance the larger net absorbed shortwave radiation and, together with the surface radiation budget, are consistent with the cooler ground temperature found in the swamp case. Note that in central Sudan and along the Sahel band, changes in latent heat flux (Fig. 13f) are up to 5 W/m^2 indicating an increase in surface evaporation, consistent with the increases of rainfall over these regions.

5.3 Impact on large-scale circulation

The impact of land cover changes on the lower level circulation is mostly localized. In fact, as shown in Fig. 14b, changing from bare desert soil to swamp induces strong horizontal wind convergence at 925 hPa around the region and divergence at 850 hPa (Fig. 14a). This pattern of horizontal wind changes is driven by a thermally induced dipole pattern in the spatial distribution of the sea level pressure changes consisting of negative anomalies in southern Sudan and positive anomalies in regions to the north (Fig. 14c, d).

To gain insights on the causes of the minor remote effect of southern Sudan land cover change over the Sahel band, we then analyze the differences between the two experiments in the dynamical features affecting both regions (East and West Africa), namely the TEJ, the AEJ, and the AEWs. These are characterized by the zonal wind differences at 150 hPa, at 600 hPa and the 2–10 days of filtered midlevel meridional wind variance (Fig. 15c). In the upper level, the easterlies increase in the swamp experiment by up to 25 cm/s over Africa (Fig. 15a) between 10 °N and 5 °S, indicating a strengthening of the TEJ. At the midlevel (Fig. 15b), weaker and stronger easterlies are simulated around 15 °N and above, respectively, suggesting a northward shift of the AEJ. This strengthening of the TEJ and the displacement toward the north of the AEJ are related to changes in the lower level temperature gradient (Thorncroft
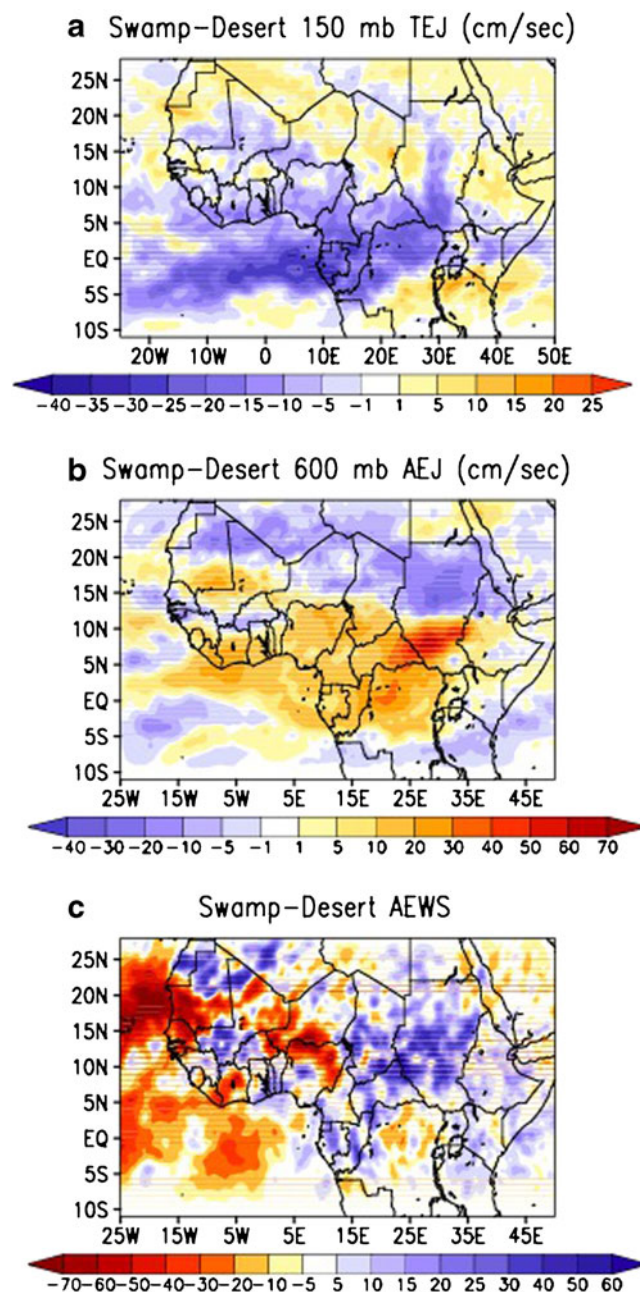
Fig. 15 Averaged zonal wind (in m/s) for JJA 1990–1999 for swamp minus bare desert soil: **a** TEJ at 150 mb, **b** AEJ at 600 mb, **c** the AEWs

and Blackburn 1999; Cook 1999; Jenkins et al. 2005; Sylla et al. 2010c) in response to the surface cooling occurring in the presence of swamp. The AEWs spatial pattern shows larger activity in the East African complex terrains, north of Sudan and over West Africa and lower activity in the adjacent Atlantic Ocean in the swamp experiment. The increase of the AEWs activity around the genesis region may be related to increased latent heating (Thorncroft et al. 2008; Leroux and Hall 2009), whereas the decrease over the Atlantic may be induced by a decrease of the deep convection (Sylla et al.

2011). The latter is consistent with the little drier conditions found in the Atlantic Ocean.

In general, the little changes in the West African summer monsoon climate induced by the swamp with respect to bare desert soil over the southern Sudan indicate more occurrences of longer lasting rain-producing systems toward the north and therefore explain the wetter climate over the north of the swamp region (Gu et al. 2004; Mohr and Thorncroft 2006; Nicholson 2008; Sylla et al. 2010a).

6 Conclusion

Wetlands are important for the carbon cycle, water balance, wildlife, biodiversity, and human food production (Neue et al. 1997); however, they can also affect climate regionally through land–atmosphere exchanges. This paper investigates the effect of swamps on the climatology of the southern Sudan and on the summer regional climates of Africa north of the equator. Towards this purpose, a series of high resolution regional climate model sensitivity experiments with different surface types (control, swamp, and bare desert soil) are conducted and intercompared. Ten summer seasons (from 1990 to 1999) are simulated for a domain covering the African continent and adjacent oceans north of 10 °S, with lateral boundary conditions from the ERA Interim reanalysis.

The RegCM3 control experiment is first evaluated against observations and the reanalysis. It is shown that the model performs reasonably well in reproducing the observed climatology of temperature, precipitation, relative humidity, and large-scale atmospheric circulation features. For example, the model captures well the rain belt and the precipitation break in the West African ITCZ, as well as the peaks in Ethiopian Highlands, Guinea Highlands, and Cameroon Highlands. In general, the temperature biases are approximately between −2 and 2 °C. Although a cold bias still dominates around the sub-equatorial regions, the new simulation outperforms the previous application of this model over the region (Sylla et al. 2010b). The spatial distribution of total cloud cover is well reproduced; however, some negative bias (about 20–25 %) prevails in the Congo basin area, leading to excessive OLR. In addition, the lower level and large-scale circulation features affecting the monsoon (TEJ, AEJ, AEWs) are realistically captured, although the model shows an overestimation of the wave's activity downstream of Ethiopian Highlands compared to the ERA Interim reanalysis.

The sensitivity experiments to land use modifications over the southern Sudan area reveal that, compared to the bare desert soil case, the swamp leads to lower surface temperature (of up to 2 °C) in the areas of the perturbation. Precipitation is locally increased over the swamp area (about 40 %) due to greater evaporation and stronger low level convergence. Although the swamp effects are mostly localized, some response is found also remotely, more specifically a minor increase of precipitation in central Sudan (about 15 %).

Our work highlights the relevant role of land surface conditions in affecting local climate of the African continent land–atmosphere interaction. It is therefore important to accurately specify and model land surface conditions and processes for an accurate simulation of possible climatic changes over the African continent. In this paper, we adopted idealized land surface change representations, and further work will attempt to utilize more realistic land surface models and conditions.

References

Adler RF, Susskind J, Huffman GJ, Bolvin D, Nelkin E, Chang A, Ferraro R, Gruber A, Xie PP, Janowiak J (2003) The version-2 global precipitation climatology project (GPCP) monthly precipitation analysis (1979–present). J Hydrometeorol 4:1147–1167

Anyah RO, Semazzi FHM (2007) Variability of East African rainfall based on multiyear RegCM3 simulations. Int J Climatol 27:357–371

Awadalla SS (2011) Wetland model in an earth systems modeling framework for regional environmental policy Analysis. Massachusetts Institute of Technology

Butcher AD (1938) The Sadd hydraulics. Govt. Press, Cairo

Chan SO, Eagleson PS (1980) Water balance studies of the Bahr El Ghazal Swamp. Dept. of Civil Engineering, Massachusetts Institute of Technology, Cambridge

Chen TC, van Loon H (1987) Interannual variation of the tropical easterly jet. Monthly Weather Review, 115

Cook KH (1999) Generation of the African easterly jet and its role in determining West African precipitation. J Clim 12:1165–1184

d'Amato N, Lebel T (1998) On the characteristics of the rainfall events in the Sahel with a view to the analysis of climatic variability. Int J Climatol 18:955–974

Dickinson RE, Henderson-Sellers A, Kennedy PJ, Wilson MF (1993) Biosphere–atmosphere transfer scheme (BATS) version 1e as coupled to the NCAR Community Climate Model. NCAR Tech. Note, NCAR/TN387+ STR

Diedhiou A, Janicot S, Viltard A, de Felice P, Laurent H (1999) Easterly wave regimes and associated convection over West Africa and tropical Atlantic: results from the NCEP/NCAR and ECMWF reanalyses. Clim Dyn 15:795–822

Druyan LM, Fulakeza M, Lonergan P (2008) The impact of vertical resolution on regional model simulation of the west African summer monsoon. Int J Climatol 28:1293–1314

Dumont HJ (2009) The Nile: origin, environments, limnology and human use. Springer, Dordrecht

Eltahir EAB (1989) A feedback mechanism in annual rainfall, Central Sudan. J Hydrol 110:323–334

Flaounas E, Bastin S, Janicot S (2010) Regional climate modelling of the 2006 West African monsoon: sensitivity to convection and planetary boundary layer parameterisation using WRF. Climate Dynamics, 1–23

Fontaine B, Janicot S (1992) Wind-field coherence and its variations over West Africa. J Clim 5:512–524

Fritsch JM, Chappell CF (1980) Numerical prediction of convectively driven mesoscale pressure systems. Part I: convective parameterization. J Atmos Sci 37:1722–1733

Gallée H, Moufouma-okia W, Bechtold P, Brasseur O, Dupays I, Marbaix P, Messager C, Ramel R, Lebel T (2004) A high resolution simulation of a West African rainy season using a regional climate model. J Geophys Res 109:D05108

Gaudet SC, Eagleson PS (1984) Surface area variability of the Bahr el Ghazal swamp in the presence of perimeter canals. Massachusetts Institute of Technology, Cambridge

Giorgi F, Bates GT (1989) The climatological skill of a regional model over complex terrain. Mon Weather Rev 117:2325

Giorgi F, Marinucci MR, Bates GT (1993) Development of a second-generation regional climate model (RegCM2). Part I: boundary-layer and radiative transfer processes. Mon Weather Rev 121:2794–2813

Green J, El-Moghraby AI (2009) Swamps of the upper White Nile. The Nile, 193-204.

Grell GA, Dudhia J, Stanffer DR (1994) A description of the fifth-generation Penn State/NCAR Mesoscale Model (MMS). NCAR Tech. Note, NCAR/TN-398+STR, 122 pp

Gu G, Adler RF, Huffman GJ, Curtis S (2004) African easterly waves and their association with precipitation. J Geophys Res 109: D04101

Holtslag AAM, de Bruijn EIF, Pan HL (1990) A high resolution air mass transformation model for short-range weather forecasting. Monthly Weather Review, 118

Hurst HE, Phillips P (1938) The Nile Basin, V, the hydrology of the Lake Plateau and Bahr el Jebel. Government Press, Cairo

Jenkins GS, Gaye AT, Sylla B (2005) Late 20th century attribution of drying trends in the Sahel from the Regional Climate Model (RegCM3). Geophys Res Lett 32:L22705

Kiehl JT, Hack JJ, Bonan GB, Boville B (1996) Description of the NCAR Community Climate Model (CCM 3). NASA, Boulder

Koteswaram P (1958) The Easterly Jet Stream in the tropics*. Tellus 10:43–57

Leroux S, Hall NMJ (2009) On the relationship between African easterly waves and the African easterly jet. J Atmos Sci 66:2303–2316

Liebmann B, Smith CA (1996) Description of a complete (interpolated) outgoing longwave radiation dataset. Bull Amer Meteor Soc 77:1275–1277

Mekonnen A, Thorncroft CD, Aiyyer AR (2006) Analysis of convection and its association with African easterly waves. J Clim 19:5405–5421

Mitchell TD, Carter TR, Jones PD, Hulme M, New M (2004) A comprehensive set of high-resolution grids of monthly climate for Europe and the globe: the observed record (1901–2000) and 16 scenarios (2001–2100). Journal of Climate.

Mohamed YA, Bastiaanssen WGM, Savenije HHG (2004) Spatial variability of evaporation and moisture storage in the swamps of the upper Nile studied by remote sensing techniques. J Hydrol 289:145–164

Mohamed YA, Van Den Hurk B, Savenije HHG, Bastiaanssen WGM (2005a) Hydroclimatology of the Nile: results from a regional climate model. Hydrol Earth Syst Sci Discuss 2:319–364

Mohamed YA, Van Den Hurk B, Savenije HHG, Bastiaanssen WGM (2005b) Impact of the Sudd wetland on the Nile hydroclimatology. Water Resour Res 41:W08420

Mohr KI, Thorncroft CD (2006) Intense convective systems in West Africa and their relationship to the African easterly jet. Q J R Meteorol Soc 132:163–176

Neue HU, Gaunt JL, Wang ZP, Becker-Heidmann P, Quijano C (1997) Carbon in tropical wetlands. Geoderma 79:163–185

Nicholson SE (2008) The intensity, location and structure of the tropical rainbelt over west Africa as factors in interannual variability. Int J Climatol 28:1775–1785

Nikulin G, Jones C, Samuelsson P, Giorgi F, Sylla MB, Asrar G, Baüchner M, Christensen OB, Déqué M, Fernandez J (2012) Precipitation climatology in an ensemble of CORDEX-Africa regional climate simulations. Journal of Climate. doi:10.1175/JCLI-D-11-00375.1

Paeth H, Born K, Podzun R, Jacob D (2005) Regional dynamical downscaling over West Africa: model evaluation and comparison of wet and dry years. Meteorol Z 14:349–368

Pal JS, Eltahir EAB, Small EE (2000) Simulation of regional-scale water and energy budgets—representation of subgrid cloud and precipitation processes within RegCM. J Geophys Res 105:567–594

Pal JS, Giorgi F, Bi X, Elguindi N, Solmon F, Rauscher SA, Gao X, Francisco R, Zakey A, Winter J (2007) Regional climate modeling for the developing world: the ICTP RegCM3 and RegCNET. Bull Am Meteorol Soc 88:1395–1409

Reynolds RW, Smith TM, Liu C, Chelton DB, Casey KS, Schlax MG (2007) Daily high-resolution-blended analyses for sea surface temperature

Ruti PM, Dell'aquila A (2010) The twentieth century African easterly waves in reanalysis systems and IPCC simulations, from intra-seasonal to inter-annual variability. Climate dynamics, 1–19.

Schuyt KD (2005) Economic consequences of wetland degradation for local populations in Africa. Ecol Econ 53:177–190

Shamseddin MAH, Hata T, Tada A, Bashir MA, Tanakamaru T (2006) Estimation of flooded area in the Bahr El-Jebel basin using remote sensing techniques. Hydrol Earth Syst Sci Discuss 3:1851–1877

Steiner AL, Pal JS, Rauscher SA, Bell JL, Diffenbaugh NS, Boone A, Sloan LC, Giorgi F (2009) Land surface coupling in regional climate simulations of the West African monsoon. Clim Dyn 33:869–892

Sun L, Semazzi FHM, Giorgi F, Ogallo L (1999) Application of the NCAR regional climate model to eastern Africa 1. Simulation of the short rains of 1988. J Geophys Res 104:6529–6548

Sutcliffe, J. V., Parks, Y. P., International Association OF Hydrological, S., Iahs & Aish (1999) The hydrology of the Nile. International Association of Hydrological Sciences, Wallingford

Sylla MB, Coppola E, Mariotti L, Giorgi F, Ruti PM, Dell'aquila A, Bi X (2010a) Multiyear simulation of the African climate using a regional climate model (RegCM3) with the high resolution ERA-interim reanalysis. Clim Dyn 35:231–247

Sylla MB, Dell'aquila A, Ruti PM, Giorgi F (2010b) Simulation of the intraseasonal and the interannual variability of rainfall over West Africa with RegCM3 during the monsoon period. Int J Climatol 30:1865–1883

Sylla MB, Gaye AT, Jenkins GS, Pal JS, Giorgi F (2010c) Consistency of projected drought over the Sahel with changes in the monsoon circulation and extremes in a regional climate model projections. J Geophys Res 115:D16108

Sylla MB, Giorgi F, Ruti PM, Calmanti S, Dell'aquila A (2011) The impact of deep convection on the West African summer monsoon climate: a regional climate model sensitivity study. Q J R Meteorol Soc 137:1417–1430. doi:10.1002/qj.853

Sylla MB, Giorgi F, Coppola E, Mariotti L (2012) Uncertainties in daily rainfall over Africa: assessment of gridded observation products and evaluation of a regional climate model simulation. Int J Climatol. doi:10.1002/joc.3551

Tate E, Sutcliffe J, Conway D, Farquharson F (2004) Water balance of Lake Victoria: update to 2000 and climate change modelling to 2100 / Bilan hydrologique du Lac Victoria: mise à jour jusqu'en 2000 et modélisation des impacts du changement climatique jusqu'en 2100. Hydrol Sci J 49:574

Teferi E, Uhlenbrook S, Bewket W, Wenninger J, Simane B (2011) The use of remote sensing to quantify wetland loss in the Choke Mountain range, Upper Blue Nile basin, Ethiopia. Hydrol Earth Syst Sci 14:2415–2428

Thorncroft CD, Blackburn M (1999) Maintenance of the African easterly jet. Q J R Meteorol Soc 125:763–786

Thorncroft CD, Hall NMJ, Kiladis GN (2008) Three-dimensional structure and dynamics of African easterly waves. Part III: genesis. J Atmos Sci 65:3596–3607

Turner RK, Van Den Bergh JCJM, Söderqvist T, Barendregt A, Van Der Straaten J, Maltby E, Van Ierland EC (2000) Ecological-economic analysis of wetlands: scientific integration for management and policy. Ecol Econ 35:7–23

Uppala S, Dee D, Kobayashi S, Berrisford P, Simmons A (2008) Towards a climate data assimilation system: status update of ERA-Interim. ECMWF Newsletter 115:12–18

Vizy EK, Cook KH (2002) Development and application of a meso-scale climate model for the tropics: influence of sea surface temperature anomalies on the West African monsoon. J Geophys Res 107:4023

Wu MLC, Reale O, Schubert SD, Suarez MJ, Koster RD, Pegion PJ (2009) African easterly jet: structure and maintenance. *Journal of Climate*, 4459–4480

Zeng X, Zhao M, Dickinson RE (1998) Intercomparison of bulk aerodynamic algorithms for the computation of sea surface fluxes using TOGA COARE and TAO data. J Clim 11:2628–2644